International Immunology, Vol. 31, No. 4, pp. 187–198
doi:10.1093/intimm/dxy079
Advance Access publication 15 December 2018

Metformin induces CD11b$^+$-cell-mediated growth inhibition of an osteosarcoma: implications for metabolic reprogramming of myeloid cells and anti-tumor effects

Takenori Uehara[1,2], Shingo Eikawa[1], Mikako Nishida[1], Yuki Kunisada[1], Aki Yoshida[2], Tomohiro Fujiwara[2], Toshiyuki Kunisada[3], Toshifumi Ozaki[2] and **Heiichiro Udono[1]**

[1]Department of Immunology,
[2]Department of Orthopaedic Surgery and
[3]Medical Materials for Musculoskeletal Reconstitution, Okayama University Graduate School of Medicine, Dentistry, and Pharmaceutical Sciences, 2-5-1 Shikata-cho, Kita-ku, Okayama 700-8558, Japan

Correspondence to: H. Udono; E-mail: udono@cc.okayama-u.ac.jp

Received 8 August 2018, *editorial decision* 14 November 2018; *accepted* 20 November 2018

Abstract

CD11b$^+$ myeloid subpopulations, including myeloid-derived suppressor cells (MDSCs) and tumor-associated macrophages (TAMs), play crucial roles in the suppression of T-cell-mediated anti-tumor immunity. Regulation of these cell types is a primary goal for achieving efficient cancer immunotherapy. We found that metformin (Met) induces CD11b$^+$-cell-mediated growth inhibition of a K7M2neo osteosarcoma independent of T cells, as growth inhibition of K7M2neo was still observed in wild-type (WT) mice depleted of T cells by antibodies and in SCID; this contrasted with the effect of Met on Meth A fibrosarcoma, which was entirely T-cell-dependent. Moreover, the inhibitory effect seen in SCID was abrogated by anti-CD11b antibody injection. PMN-MDSCs were significantly reduced in both spleens and tumors following Met treatment. In TAMs, production of IL-12 and TNF-α, but not IL-10, became apparent, and elevation of MHC class II with reduction of CD206 was observed, indicating a shift from an M2- to M1-like phenotype via Met administration. Metabolically, Met treatment decreased basal respiration and the oxygen consumption rate (OCR)/extracellular acidification rate (ECAR) ratio of CD11b$^+$ cells in tumors, but not in the spleen. In addition, decreased reactive oxygen species (ROS) production and proton leakage in MDSCs and TAMs were consistently observed in tumors. Uptake of both 2-deoxy-2-D-glucose (2-NBDG) and BODIPY® decreased in MDSCs, but only BODIPY® incorporation was decreased in TAMs. Overall, our results suggest that Met redirects the metabolism of CD11b$^+$ cells to lower oxidative phosphorylation (OXPHOS) while elevating glycolysis, thereby pushing the microenvironment to a state that inhibits the growth of certain tumors.

Keywords: immunometabolism, myeloid-derived suppressor cells (MDSCs), tumor-associated macrophages (TAMs), tumor immunity, tumor microenvironment

Introduction

The tumor microenvironment is composed of myeloid cells, including myeloid-derived suppressor cells (MDSCs) and tumor-associated macrophages (TAMs). MDSCs and immunosuppressive TAMs stimulate the differentiation and homing of regulatory T cells (Tregs) to tumors (1). These cell components have been implicated as the main negative regulators of T-cell-mediated anti-tumor immunity (2–4). Therefore, targeting myeloid cells in tumors could be an attractive approach as a part of combination therapy against cancers. MDSCs form a heterogeneous population that includes morphologically monocytic (M)-MDSCs and granulocytic polymorphonuclear (PMN)-MDSCs with multilobed nuclei, which are phenotypically characterized as CD11b$^+$Ly6G$^-$Ly6C$^+$ or CD11b$^+$Ly6G$^+$Ly6C$^-$, respectively (5–7). The presence of tumors partially blocks the differentiation of immature myeloid cells in the bone marrow into becoming macrophages,

neutrophils or dendritic cells, which results in expansion of the MDSC population in the peripheral blood (2). Hypoxic conditions within tumors facilitate the homing of myeloid cells into tumor tissues (8). The suppressive mechanisms of MDSCs are associated with a number of factors, including reactive oxygen species (ROS), inducible nitric oxide synthase (iNOS) and arginase, all of which are involved in the suppression of T-cell function (9, 10). Cyclooxygenase-2 and prostaglandin E2 (PGE2) are produced by tumors, which in turn activate MDSCs to express arginase, iNOS and PGE2 (11, 12).

Macrophages are heterogeneous cell populations with diverse immunological functions. However, they are commonly classified as simply M1 (activated) or M2 (alternatively activated), due to the usefulness of these terms in understanding inflammatory and anti-inflammatory (i.e. wound healing) states, respectively (13, 14). TAMs are closely related to the M2 subset and exhibit protumorigenic properties via stimulation of the angiogenic process through the secretion of proangiogenic cytokines, such as vascular endothelial growth factor (15, 16), as well as by suppression of tumor antigen-reactive T cells through the production of immune suppressive cytokines, such as interleukin-10 (IL-10) (17, 18). Therefore, TAM accumulation in tumors is predictive of poor prognoses in cancer patients (19, 20). In contrast, M1-like macrophages direct tumor resistance through the secretion of tumoricidal cytokines, such as tumor necrosis factor-alpha (TNF-α) and IL-12. On the basis of this theoretical framework, targeting TAMs either by depletion or repolarization could be an ideal therapeutic intervention for cancers. Moreover, the inhibition of colony-stimulating factor (CSF) signaling through anti-CSF1 receptor-neutralizing antibodies or chemical compound inhibitors has been reported to reduce tumor volume in mice by repolarization of TAMs to anti-tumoral macrophages (i.e. an M1-like phenotype) (21–24).

Metabolism in innate immune cells, as well as T cells, is tightly coupled with cell function and differentiation (25). For example, in M1-like macrophages, lipopolysaccharide (LPS) and type I interferon (IFN) stimulation induces a metabolic switch from oxidative phosphorylation (OXPHOS) to glycolysis, with a resulting decrease in tricarboxylic acid (TCA) cycle activity (26, 27). In contrast, M2-like macrophages exhibit increased OXPHOS and secrete IL-10 while decreasing the production of TNF-α (28, 29). Certain drug-induced metabolic reprogramming of myeloid cells might affect their suppressive tumor immunity properties. We found previously that the type 2 diabetes drug metformin (Met) helped tumor-infiltrating CD8 T lymphocytes (CD8TILs) recover from exhaustion, which was followed by growth inhibition of several tumors in syngeneic mouse models (30). The CD8TIL phenotype was shifted from $CD44^{+}CD62L^{high}$ central memory T cells to $CD44^{+}CD62L^{low}$ effector memory cells, suggesting that Met induced metabolic reprogramming toward glycolysis rather than OXPHOS. In addition, we found that Met attenuated Treg differentiation in tumors through the activation of mTORC1, which was also accompanied by elevation of glycolysis in Tregs (31). In light of our previous observations, the purpose of the present study was to determine whether Met influences the generation and function of $CD11b^{+}$ myeloid cells, especially MDSCs and TAMs, in a K7M2neo mouse osteosarcoma model. We found that Met-dependent osteosarcoma growth inhibition was still observed in SCID mice, and that anti-CD11b antibody injection abrogated this effect. However, this was not always the case, as Met-induced growth inhibition of Meth A, a fibrosarcoma model, was never observed in SCID mice. Additionally, we found that Met reduced the MDSC numbers in spleens and tumors, particularly PMN-MDSCs, and that Met reduced M2-like macrophage numbers exhibiting an MHC class II^{low}, $CD206^{high}$ phenotype. These phenotypic alterations were found to be associated with metabolic changes in $CD11b^{+}$ cells that were down-regulated in OXPHOS, as determined by experiments with a Seahorse Analyzer and ROS production, as well as by the observed incorporation of 2-deoxy-2-D-glucose (2-NBDG) and BODIPY®.

Methods

Mice

BALB/c wild-type (WT) mice and BALB/c SCID mice were purchased from SLC and CLEA, Japan. All mice were maintained under specific pathogen-free conditions in the animal facility of Okayama University. The Institutional Animal Care and Use Committee of Okayama University Graduate School of Medicine approved the studies.

Tumor cell lines

A BALB/c osteosarcoma cell line K7M2-pCI Neo (K7M2neo) was purchased from ATCC and used for the tumor assays. Cells were cultured in Dulbecco's modified Eagle's medium with 4 mM L-glutamine adjusted to contain 1.5 g l^{-1} sodium bicarbonate and 4.5 g l^{-1} glucose (Wako Pure Chemical Industries, Ltd, Osaka, Japan) and supplemented with 0.8 mg ml^{-1} G-418 (Roche, Mannheim, Germany), 10% fetal bovine serum and 10 μM 2-mercaptoethanol.

Cell proliferation assay

Osteosarcoma cells were seeded in 96-well flat-bottom plates at 5×10^3 cells per well with 100 μl of culture medium (described above). The cells were cultured for 48 h, and then 10 μl of Cell Proliferation Reagent WST-1 (Roche) was added. After 120 min, the absorbance of the culture medium at 450 nm was measured using a microplate reader (DS Pharma Biomedical, Osaka, Japan).

Tumor growth assay

Mice were intra-dermally inoculated in the back flank (right side) with 4×10^5 K7M2neo cells using a 27-gauge needle. Subsequently, mice were orally administered 5 mg ml^{-1} of metformin hydrochloride (Tokyo Chemical Industry Co., Ltd, Japan) dissolved in free drinking water. To deplete T cells *in vivo*, 50 μl ascites formed with antibodies against CD4 and CD8 molecules was diluted in 150 μl phosphate-buffered saline (PBS) and injected into mice from day 7 at 4-day intervals, as described previously (30). To deplete $CD11b^{+}$ cells *in vivo*, 100 μg anti-CD11b antibody (5C6 clone 1, BioGate Co., Ltd, Gifu, Japan) was injected in 5-day intervals throughout the experiments. The long (*a*) and short (*b*) tumor diameters were measured using Vernier calipers, while tumor volume (*V*) was calculated according to the following equation: $V = a \times b^2/2$.

Isolation of tumor-associated myeloid cells

Tumor tissues were dissected from mice and minced into small pieces in PBS buffer. Cells were isolated using a Medimachine system (AS ONE, Osaka, Japan). Isolated cells, including tumor-infiltrating leucocytes, were then stained with the indicated fluorescence-labeled antibodies and subjected to flow cytometric analysis.

Flow cytometric analysis

Cells were incubated with a Zombie Aqua™ Fixable Viability Kit for dead cell detection, in accordance with the manufacturer's instructions. After washing with PBS, cells were incubated with monoclonal antibodies (mAbs) for 30 min at 4°C in a fluorescence-activated cell sorting (FACS) staining buffer (PBS containing 5 mM ethylenediaminetetraacetic acid and 2% fetal bovine serum). The following mAbs (BioLegend, San Diego, CA, USA) were used for cell surface marker staining: BV421™ anti-mouse CD11b, PerCP Cy5.5 anti-mouse CD11b, PE anti-mouse Gr-1(Ly-6G/C), PE-Cy7 anti-mouse Ly-6G, APC-Cy7 anti-mouse Ly-6C, PerCP Cy5.5 anti-mouse CD45.2, PE-Cy7 anti-mouse F4/80, FITC anti-mouse F4/80, APC anti-mouse CD3, FITC anti-mouse I-A/I-E, APC anti-mouse CD206 and FITC anti-mouse NKp46. For cytokine staining of tumor-associated macrophages, on day 22 after tumor inoculation, the tumor-derived cells were incubated with LPS (1 μg ml^{-1}) and IFN-γ (10 ng ml^{-1}) for 24 h. The resulting cells were further stimulated with LPS (1 μg ml^{-1}) and IFN-γ (10 ng ml^{-1}) and IL-4 (10 ng ml^{-1}) in the presence of Monensin for 6 h, and then stained with antibodies to cytokines. FITC anti-mouse IL-10, APC anti-mouse IL-12/IL-23p40 and BV421 anti-mouse TNF-α were used for intracellular cytokine staining. Intracellular cytokine staining was performed with a fixation/permeabilization kit (BD Biosciences). After staining, cells were washed and suspended in FACS buffer and analyzed with a FACSCanto II flow cytometer (BD Biosciences).

Intracellular ROS production

Cell suspensions from Met-treated or untreated tumor-bearing mice were plated on a 12-well culture plate at 1 × 10^6 cells per ml in culture medium. After surface marker staining as described above, the cells were incubated with 20 μM 2′,7′-dichlorofluorescein diacetate (DCFDA, Abcam plc, Cambridge, UK) for 20 min at 37°C. The cells were washed once with FACS buffer, and DCFDA fluorescence was measured using a FACSCanto II.

Metabolic assays

Splenocytes and tumor cells harvested from tumor-bearing mice were stained with PE anti-mouse CD11b. CD11b$^+$ cells were isolated using anti-PE magnetic beads, and then the sorted CD11b$^+$ cells were incubated in XF medium (non-buffered RPMI 1640 containing 25 mM glucose, 2 mM L-glutamine and 1 mM sodium pyruvate). Reagents were added to the media with the following concentrations: 1 μM oligomycin (Sigma-Aldrich, Kanagawa, Japan), 10 μM FCCP (Sigma-Aldrich) and 1 μM rotenone (Sigma-Aldrich) + 1 μM antimycin A (Sigma-Aldrich). Then oxygen consumption rates (OCRs) and extracellular acidification rates (ECARs) were measured using an XFe96 Extracellular Flux Analyzer (Seahorse Bioscience, North Billerica, MA, USA) and the XF Cell Mito Stress Test protocol. Spare capacity and proton leakage were calculated according to the following formulas:

$$\text{Spare respiratory capacity} = \text{maximal respiration} - \text{basal respiration}.$$

$$\text{Proton leak} = \text{basal respiration} - (\text{ATP production} + \text{non-mitochondrial respiration}).$$

Glucose and lipid uptake

Tumor-associated myeloid cells were harvested from tumor-bearing mice on day 36 as described above. The cells were incubated with 100 μM 2-NBDG (Thermo Fisher Scientific Inc., Waltham, MA, USA) at 37°C for 15 min. After washing, cells were incubated on ice for 15 min with 100 μM BODIPY® lipid probe (BODIPY™ 500/510 C1, C12; Thermo Fisher Scientific Inc.). After surface staining as described above, the fluorescence of 2-NBDG and BODIPY® in MDSCs and macrophages was measured using a FACSCanto II.

Statistical evaluation

Statistical analyses were performed using GraphPad Prism 6 (GraphPad Software, Inc., San Diego, CA, USA). The Student's *t*-test was used for statistical evaluations of normally distributed data. Tumor growth assays were analyzed using two-way repeated measures of analysis of variance (ANOVA) with Tukey's *post hoc* test. Cell proliferation assays and chronological changes in the percentage of lymphocytes and myeloid cells were examined using one-way ANOVA.

Results

Met-induced growth inhibition of K7M2neo osteosarcoma in WT mice

K7M2neo osteosarcoma cells originating from BALB/c mice were inoculated into the backs of syngeneic WT mice. Met dissolved in water was given starting at day 7 until the end of the experiments, and subsequent tumor growth was monitored. Growth inhibition was apparent in mice receiving Met (Fig. 1A). We checked the appearance and weight of tumors on day 35 following surgical excision and confirmed growth inhibition by Met treatment (Fig. 1B). Spleens were also harvested, and their appearance and weights were examined. The spleens in tumor-bearing mice that did not receive Met were larger, while reductions in size and weight were apparent in the Met-treated group (Fig. 1C). To check for a direct effect of Met against K7M2neo osteosarcoma cells, we co-cultured the cells with graded Met doses for 3 days, and the resulting cell proliferation was examined with a colorimetric method. Met at concentrations of 10 mM caused significant tumor inhibition, whereas doses under 5 mM never suppressed proliferation (Fig. 1D). The *in vivo* Met concentration in our experimental setting was typically ≤10 μM (32); therefore, a direct inhibitory effect on the tumor growth is unlikely.

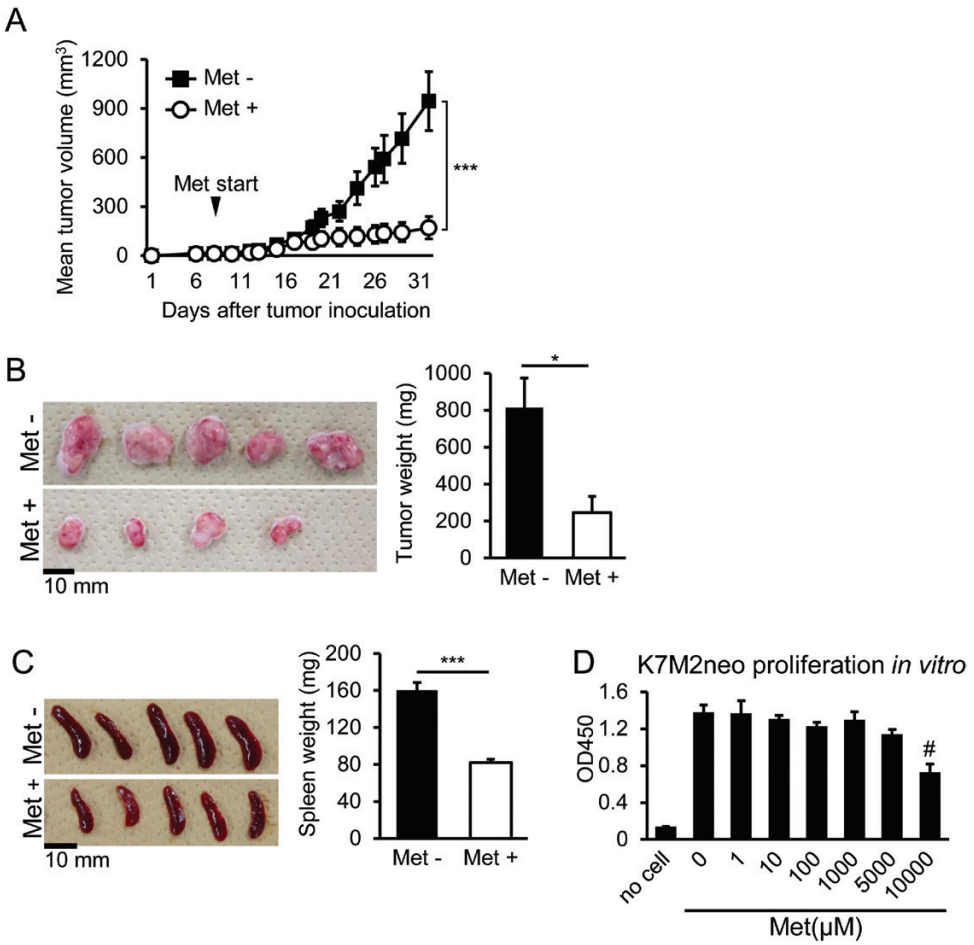

Fig. 1. Met-dependent growth inhibition of K7M2neo osteosarcoma cells *in vivo*. (A) Met significantly blocks the growth of K7M2neo osteosarcoma in syngeneic WT mice. Met administration was commenced on day 7 following tumor challenge, and subsequent growth was monitored. The results are shown as mean tumor volumes ± standard error of the mean (SE) ($n = 6$), and are representative of three independent experiments. (B) Surgical removal of tumors from mice on day 35 in (A) the left panel, with their weights shown in the right panel. One tumor from the Met (+) group ($n = 5$) could not be obtained as it had completely regressed. (C) The spleens of mice on day 35 in (A) are shown in the left panel with their weights in the right panel. Enlarged spleens of tumor-bearing mice were reduced in size by Met administration. (D) *In vitro* proliferation of K7M2neo cells. Cells were cultured in the presence of graded doses of Met, and proliferation was determined on day 3. Data are shown as the mean ± SE ($n = 5$). The results are representative of two independent experiments. $^{*}P < 0.05$; $^{***}P < 0.001$ by Student's *t*-test (B and C) or two-way ANOVA (A). $^{\#}P < 0.05$ by one-way ANOVA (D).

Met-induced growth inhibition of K7M2neo osteosarcoma in SCID mice

We next examined whether the Met-induced growth inhibition of K7M2neo cells was dependent on T cells by injection of antibodies against $CD8^+$ and/or $CD4^+$ T cells. We simultaneously performed the same experiments with the control tumor, Meth A fibrosarcoma cells. To our surprise, the depletion of both $CD8^+$ and $CD4^+$ T cells gave rise to only partial growth restoration in K7M2neo tumors, but resulted in complete restoration of Meth A tumors (Fig. 2A and B). Moreover, the same effects were also observed in SCID mice (Fig. 2C and D). These results raised the possibility of the involvement of non-T-cell-mediated anti-tumor factors against K7M2neo cells, in addition to $CD8^+$ T cells. One candidate for non-T-cell effectors might be $CD11b^+$ cells harboring macrophages. Since it is difficult to examine the role of TAMs as effector cells, we attempted to directly investigate whether $CD11b^+$ cells play a role as growth inhibition effector cells in SCID mice. We injected anti-$CD11b^+$ antibodies from days 19 to 34 at 5-day intervals, during which the Met-induced anti-tumor effect was apparent, and found that anti-CD11b antibodies completely abrogated growth inhibition (Fig. 3A), which suggests that the Met-induced effector cells are a $CD11b^+$ population in SCID mice. This evidence excluded the possible involvement of natural killer (NK) cells as effectors against K7M2neo. We also observed no increase in NK cell numbers in tumors upon Met treatment (Supplementary Figure 1).

Met-induced phenotypic changes of MDSCs and TAMs in tumors

Enlarged spleens, such as those found in the tumor-bearing mice (Fig. 1C), are typically caused by the accumulation of $CD11b^+$ myeloid cells (6). In our osteosarcoma model, $CD11b^+$ cells were also likely to be involved in the action of effector cells in WT mice depleted of both CD8 and CD4 T cells, as shown in Fig. 2(A). Therefore, we further examined

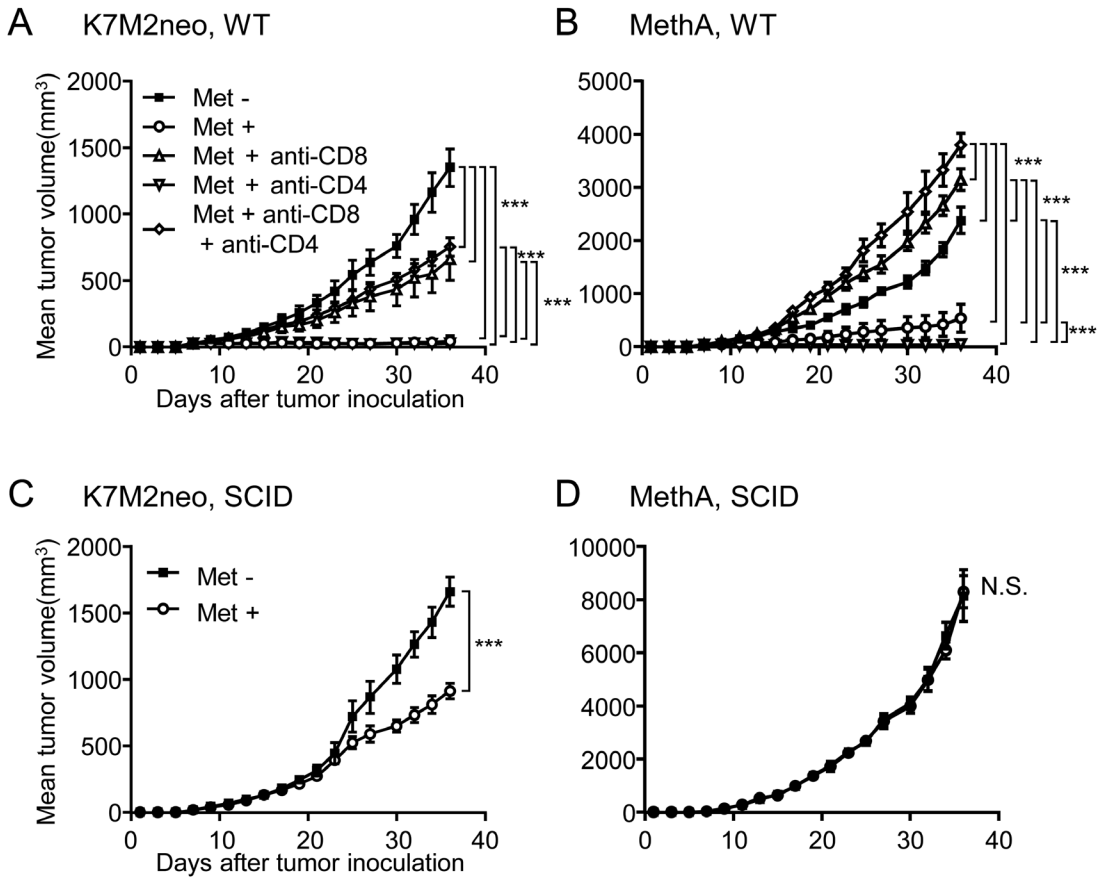

Fig. 2. Met-induced T-cell-independent growth inhibition in K7M2neo osteosarcomas. (A and B) WT mice inoculated with K7M2neo cells (A) or Meth A cells (B) were either untreated or administered Met on day 7, and injected with antibodies on the same day as indicated. Antibody injection was performed on day 7 and day 11. The results are shown as mean tumor volumes ± SE of three independent experiments (n = 6). Met-induced growth inhibition was not completely ameliorated by injection of anti-CD8 antibody in K7M2neo (A), but was completely resolved with Meth A (B). BALB/c SCID mice inoculated with K7M2neo (C) or Meth A cells (D) were untreated or administered Met on day 7, and growth was subsequently monitored. The results are shown as mean tumor volumes ± SE of two independent experiments (n = 6). Met-induced growth inhibition was observed in K7M2neo, but not in Meth A. ***P < 0.001 by two-way ANOVA.

the CD11b$^+$ myeloid cells and found that Met treatment significantly decreased CD11b$^+$ cell numbers in both the spleens and tumors of K7M2neo-bearing mice compared with untreated controls (Fig. 3B). Among myeloid cells, MDSCs and TAMs are implicated as negative regulators in T-cell-mediated anti-tumor immunity. In light of this concept, we first investigated PMN- and M-MDSC populations in spleens and tumors. A gating strategy to isolate MDSCs was developed (Fig. 4A and B). A significant decrease in PMN-, but not in M-MDSC, populations was found in both spleens and tumors following Met treatment, particularly in the late-stage tumor progression from days 29 to 36 (Fig. 4C and D). We also discovered that MHC class II I-A/I-E on PMN-MDSCs (defined as CD11b$^+$Gr-1^{high} cells) was apparently elevated by Met treatment in tumors, but not in spleens (Supplementary Figure 2).

We next focused on TAMs potentially influenced by Met treatment. TAMs were identified as a CD11b$^+$Gr1^{low} F4/80^{high} population (33, 34), as indicated in Fig. 5(A). This population did not change in tumors through Met treatment. To functionally evaluate TAMs, we stimulated the cells with LPS and examined the production of IL-10, IL-12 and TNF-α. IL-10 was dominantly produced in TAMs derived from mice that did not receive Met, whereas IL-12 and TNF-α levels were increased with Met administration (Fig. 5B and C). These results strongly indicate that TAMs were skewed to an M1-like phenotype via Met administration. Next, we tried to detect the phenotypic change of TAMs. The macrophages with lower MHC class II expression were implicated as being an immune suppressive phenotype (35). In this regard, we found significant elevation of MHC class II I-A/I-E by Met treatment (Fig. 5D), suggesting that the suppressive function might be compromised. Additionally, macrophages with a CD206^{high} phenotype have been referred to as M2-like macrophages (36, 37), and we found that the CD206 expression level was significantly decreased upon receiving Met treatment (Fig. 5D and E). In addition, it has been suggested that the anti-tumor effect of Met might be caused by anti-angiogenic activities through macrophage polarization into an M1-like phenotype (38). This observation is consistent with our conjecture. Overall, it is reasonable to postulate that the immune suppressive effect of TAMs is blunted, and in addition, increased numbers of M1-like macrophages play a critical role in growth inhibition of osteosarcomas with Met treatment.

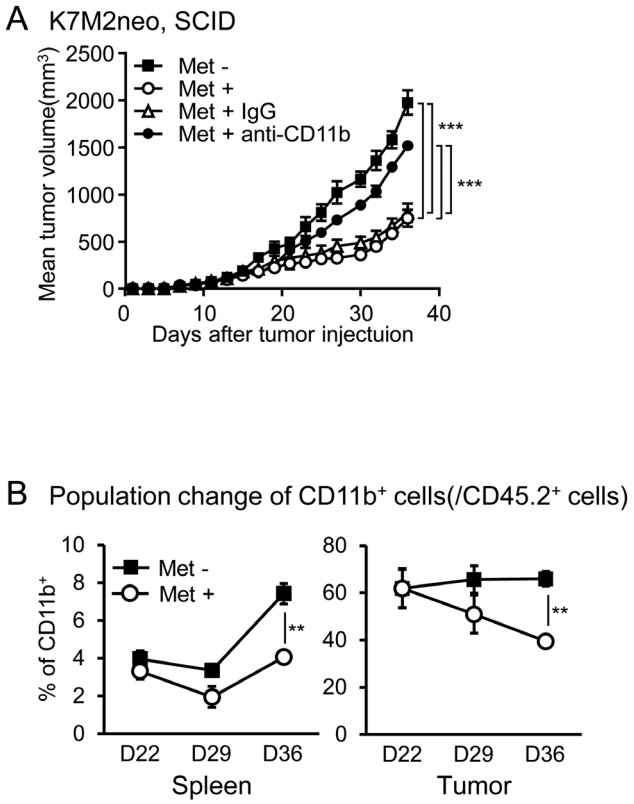

Fig. 3. Met-induced growth inhibition of K7M2neo is dependent on CD11b$^+$ cells. (A) BALB/c SCID mice inoculated with K7M2neo cells were untreated or administered Met on day 7 and injected with the indicated antibodies from days 19 to 34 at 5-day intervals. Results are shown as the mean tumor volumes ± SE of two independent experiments (n = 5). Of note, anti-CD11b antibody injection completely abrogated Met-induced growth inhibition of K7M2neo. ***$P < 0.001$ by two-way ANOVA. (B) The ratio of CD11b$^+$ cells/CD45.2$^+$ cells was examined in spleens and tumors as indicated. Animals were either untreated or given Met starting on day 7. **$P < 0.01$ by Student's t-test.

Metabolic profile of CD11b$^+$ cells including MDSCs and TAMs

MDSCs utilize ROS as effector molecules for suppression of T-cell-mediated immunity. Additionally, ROS production is implicated as a biological marker of mitochondrial respiration. However, we found a significant reduction of ROS levels with Met treatment in both MDSCs and CD11b$^+$Gr-1^{low} F4/80^{high} TAMs in tumors, but not in spleens (Fig. 6A–C). We further investigated the metabolic profile of CD11b$^+$ cells isolated from the spleens and tumors of mice and noted that spare respiratory capacity (SRC) was apparently enhanced by Met treatment in CD11b$^+$ cells in spleens, but not in tumors (Supplementary Figure 3; Fig. 6D and E). In contrast, basal respiratory capacity (BRC) was significantly down-regulated in CD11b$^+$ cells in tumors, but not in spleens (Fig. 6D and E). Thus, the metabolic profiles detected by the Seahorse Analyzer were dependent on the tissues in which the myeloid cells were located. Decreased proton leak was apparent in CD11b$^+$ cells in tumors (Fig. 6E), which is likely to be associated with the down-regulation of ROS production in those cells. Importantly, ECARs were unaltered by Met treatment in the myeloid cells of spleens and tumors (Fig. 6D, lower panels), suggesting that the reduced ratio of OCR to ECAR in CD11b$^+$ tumor cells was caused by decreased basal OCR and not by increased glycolysis (Fig. 6E). Concerning metabolism, dependency on OXPHOS or glycolysis has been implicated as a hallmark of M2- and M1-like macrophages, respectively (26–29). Therefore, the reduction of BRC, and hence a relative elevation of glycolysis, is likely to be associated with the phenotypic shift from M2- to M1-like macrophages in tumors.

Effects of Met on the uptake of 2-NBDG and BODIPY® by MDSCs and TAMs

Mitochondrial basal respiration was significantly decreased in CD11b$^+$ myeloid cells in the tumors of mice treated with Met (Fig. 6E). However, myeloid cells are extremely heterogeneous populations. Therefore, in order to dissect the metabolic profiles of more specific cells, we next investigated the uptake of 2-NBDG and BODIPY® by MDSCs and TAMs through flow cytometry-based analysis. We found that the incorporation of 2-NBDG and BODIPY® was decreased in both PMN- and M-MDSCs (Fig. 7A and B), suggesting that both cell types existed in a lower energetic quiescent state after Met treatment. In contrast, the uptake of 2-NBDG did not change, whereas that of BODIPY® was decreased significantly in TAMs following Met administration (Fig. 7A and B). On the basis of these data, the decreased OCR/ECAR ratio of CD11b$^+$ cells in tumors observed in Fig. 6(E) is caused by the down-regulation of OXPHOS, at least in part, and hence fatty acid oxidation (FAO) in MDSCs and TAMs. In contrast to MDSCs and TAMs, we observed no significant change in the uptake of 2-NBDG and BODIPY® by tumor cells (Supplementary Figure 4).

Discussion

In this study, we show that Met induces a reduction of PMN-MDSCs and a shift of TAMs from an M2- to M1-like phenotype within the tumor microenvironment, which may, at least in part, partially contribute to significant growth inhibition of K7M2neo osteosarcomas in a T-cell-independent manner. It remains unclear how such a change in MDSCs and TAMs influences T-cell-dependent immunity. Met-induced phenotypic alteration of MDSCs and TAMs are associated with metabolic changes of those cells resulting in the down-regulation of FAO. This observation, along with the T-cell-dependent anti-tumor effect, strongly suggests a potentially promising immunotherapy outcome against osteosarcomas. Although a combination of surgery and chemotherapy improved the prognosis of osteosarcoma patients, those with metastases or recurrent tumors are often not helped by such therapies (39). Therefore, alternative effective approaches, such as immunotherapy via administration of metformin in this study, are urgently needed for treatment of osteosarcoma.

Recently, Gordon *et al.* demonstrated that the major TAM population also expresses PD-1 (40), an immune checkpoint protein that is usually up-regulated in T cells in tumors. PD-1$^+$ TAMs were shown to express CD206^{high}, which is found in M2-like macrophages. PD-L1 expressed in tumors interacts with PD-1 on T cells and leads to T-cell immune tolerance. The

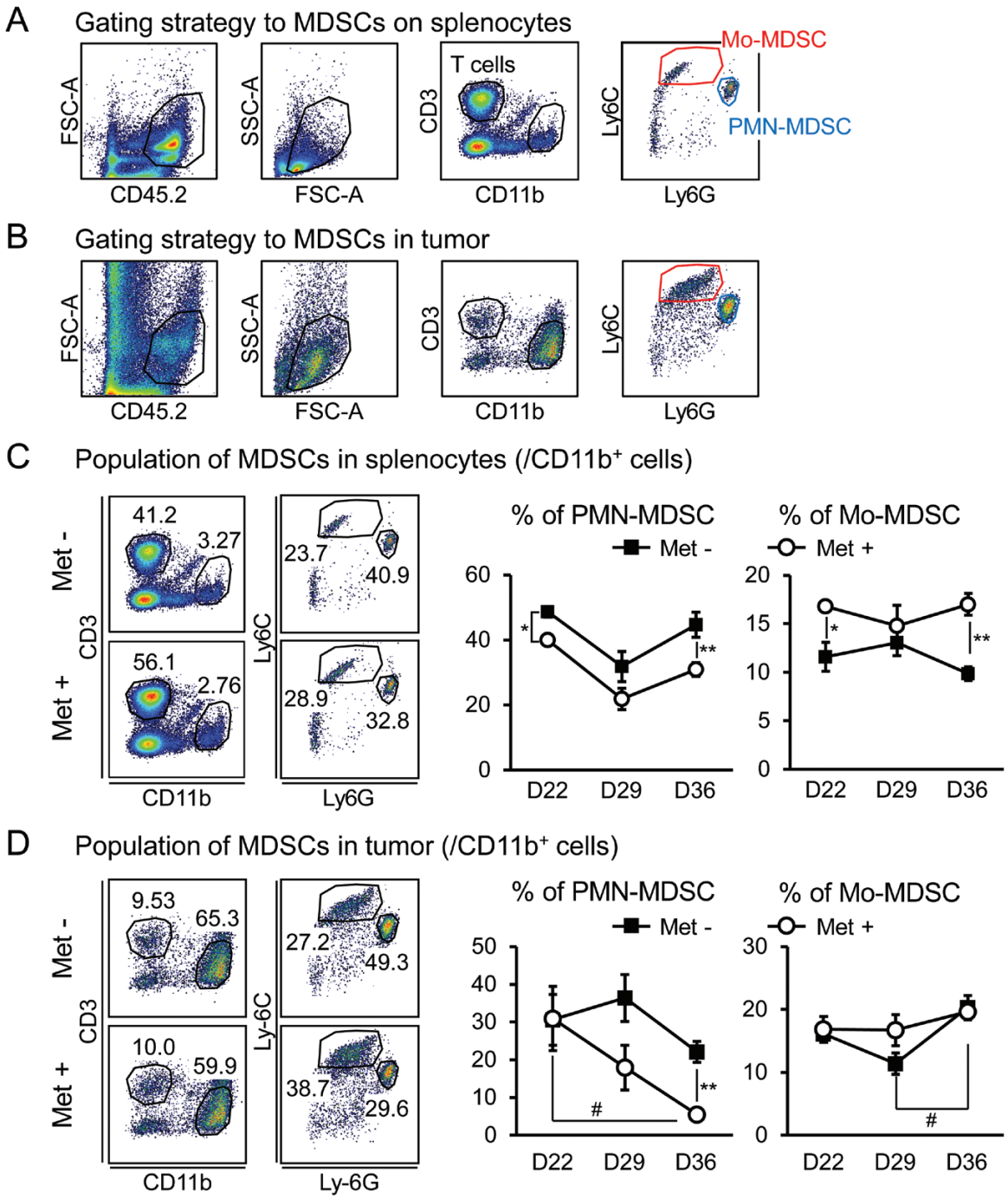

Fig. 4. Decrease in PMN-MDSCs in spleens and tumors upon Met administration. The gating strategy to identify MDSCs in spleens (A) and tumors (B). PMN- and M-MDSCs were identified as $CD11b^{+}Ly6C^{mid}Ly6G^{high}$ and $Ly6C^{high}Ly6G^{mid}$, respectively. The ratio of MDSCs to $CD11b^{+}$ cells was monitored in spleens (C) and tumors (D) over time ($n = 5$). The results are representative of four independent experiments. $^{*}P < 0.05$; $^{**}P < 0.01$ by Student's *t*-test (C and D). $^{\#}P < 0.05$ by one-way ANOVA (D).

authors showed that blockade of PD-1 on TAMs, which led to the stimulation of phagocytic functions, prolonged the survival of Rag2-deficient mice bearing CT26 colon carcinomas in a macrophage-dependent fashion (40). This T-cell-independent anti-tumor effect is very similar to our observations. In this context, whether TAM PD-1 expression is decreased in mice treated with Met remains to be investigated.

Met inhibits mitochondrial respiration of tumors. Thus, tumor-mediated oxygen consumption is also reduced, leading to reoxygenation of the tumor microenvironment. Recent findings by Scharping *et al.* suggest that the reduction of tumor hypoxia by Met potentiates the efficacy of the PD-1 blockade (41). Proliferation, IFN-γ production and cytotoxicity of activated CD8 T lymphocytes were indeed lower during

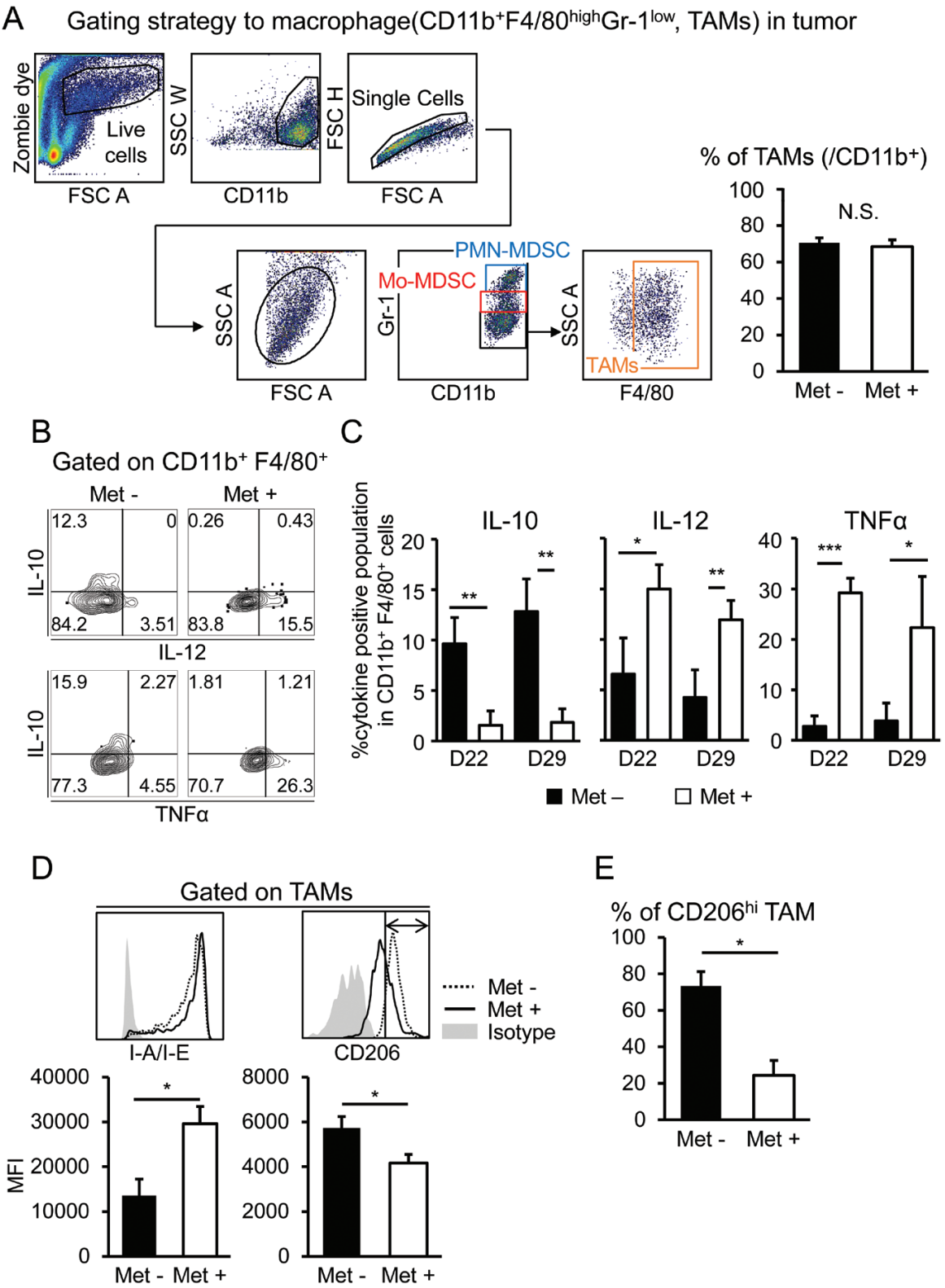

Fig. 5. Phenotypic changes of TAMs upon Met administration. (A) The gating strategy to identify TAMs in K7M2neo tumors. $CD11b^{+}Gr\text{-}1^{low}$ $F4/80^{high}$ population was identified as TAMs. (B and C) Production of intracellular cytokines, including IL-10, IL-12/IL-23p40 and TNF-α, of $CD11b^{+}F4/80^{+}$ cells was investigated after stimulation of TILs with LPS and IFN-γ for 24 h. The flow cytometry data of the pooled TILs of five mice are shown (B). Cytokine levels of $CD11b^{+}F4/80^{+}$ cells from five independent mice were tabulated as shown (C). (D) TAMs of K7M2neo-bearing mice that were untreated or administered Met were identified as in (A). Cell surface expression of MHC class II I-A/I-E and CD206 are shown as histograms with tabulation data (n = 3). The results are representative of three independent experiments. (E) The $CD206^{high}$ TAMs population was plotted as a bar graph. Note that Met treatment significantly decreased the $CD206^{high}$ population. $^{*}P < 0.05$; $^{**}P < 0.01$; $^{***}P < 0.001$ by Student's t-test.

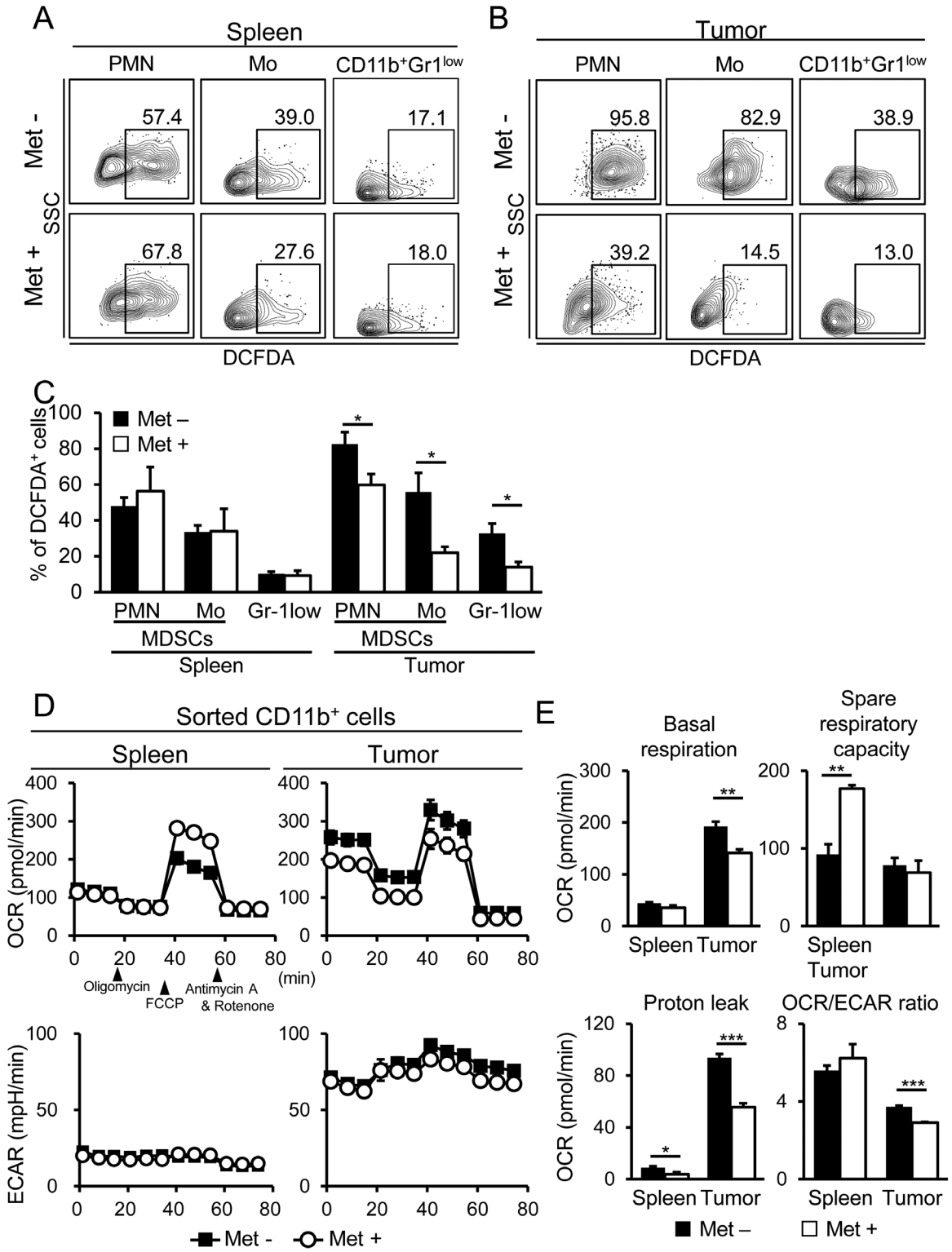

Fig. 6. Decreased OXPHOS was observed within tumor myeloid cells, but not in spleens, following Met administration. (A–C) On day 36, the percent of the DCFDA$^+$ population was determined for MDSCs and TAMs in spleens (A) and K7M2neo tumors (B) of mice that received Met or that were untreated. Flow cytometry data were obtained from pooled cells of five mice in each +/– Met group (A and B). The tabulated data are from five mice in each +/– Met group (C). Results are representative of three independent experiments. (D) The OCR and ECAR of CD11b$^+$ cells isolated from spleens and tumors were determined as indicated. The pooled cells from five mice in each +/– Met group were used for Seahorse Analyzer experiments. The results are representative of two independent experiments. (E) Basal OCR, proton leak and SRC of CD11b$^+$ cells in (D) are tabulated. Additionally, the basal OCR/ECAR ratios of splenic and tumor-infiltrating CD11b$^+$ cells are shown as a bar graph ($n = 5$). The results are representative of two independent experiments. *$P < 0.05$; **$P < 0.01$; ***$P < 0.001$ by Student's *t*-test.

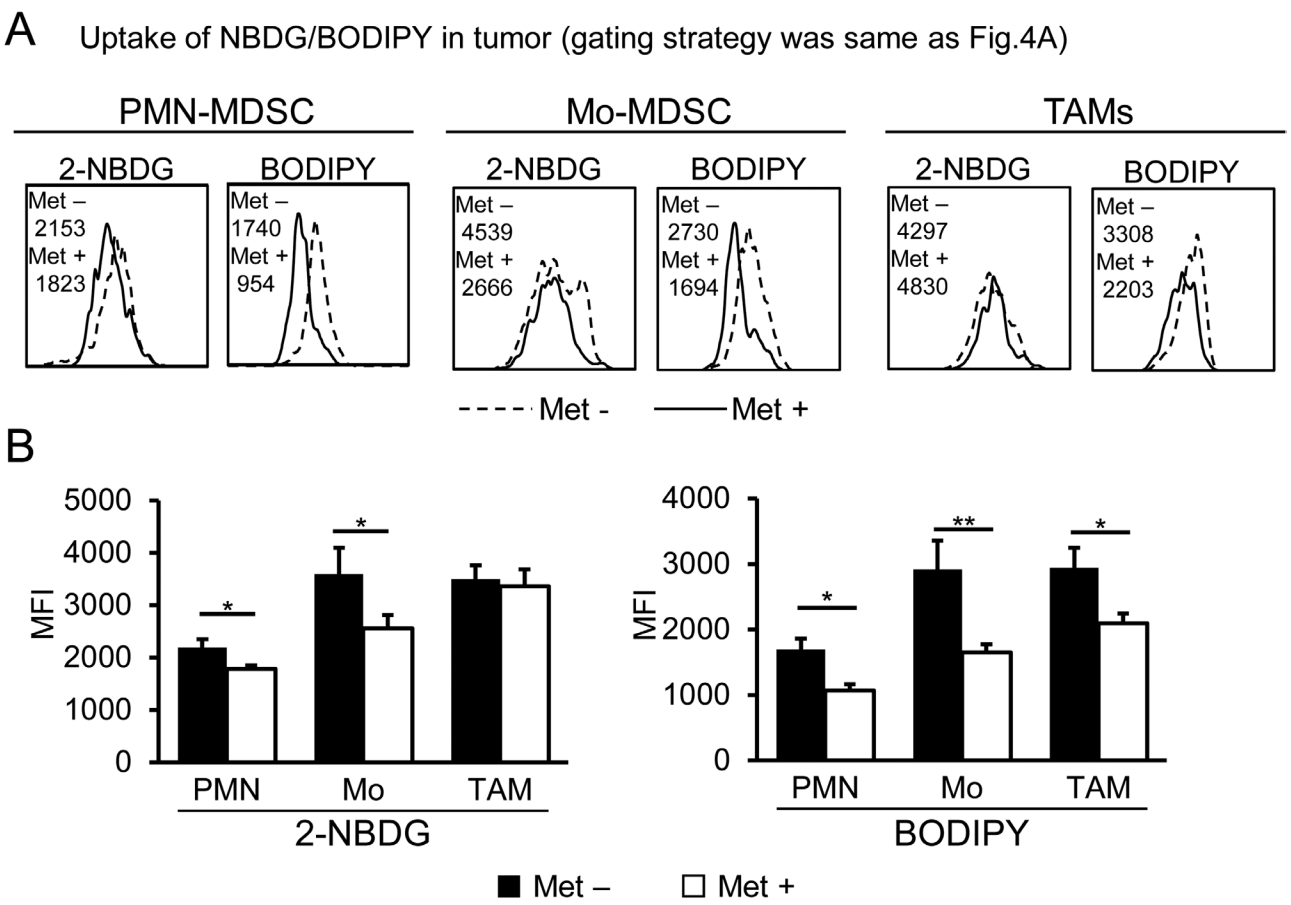

Fig. 7. Differential incorporation of 2-NBDG and BODIPY® by MDSCs and TAMs upon Met administration. On day 36, the uptake of 2-NBDG or BODIPY® by MDSCs and TAMs was examined. (A) Flow cytometry data were obtained from pooled cells from five mice in each +/– Met group. (B) Tabulated data were obtained from five mice in each +/– Met group from (A). The uptake of both 2-NBDG and BODIPY® decreased in MDSCs, but only BODIPY® incorporation decreased in TAMs upon Met administration. The results are representative of three independent experiments. *$P < 0.05$; **$P < 0.01$ by Student's *t*-test.

average tumor hypoxia (1.5% O_2) than under normoxic (21% O_2) conditions. Tumor hypoxia may affect macrophages localization in the tumor microenvironment. M1-like macrophages localize to normoxic tumor tissue, whereas hypoxic tumor tissue expresses M2 markers with proangiogenic functions (42). Our observation that M1-like macrophages are increased by Met treatment could be explained by the reoxygenation of tumors with Met.

Recent findings have suggested a link between Met and MDSCs from different perspectives. For example, Met reduces the expression of CD39 and CD73 in MDSCs, and mitigates the suppressing function of cells in patients with ovarian cancer (43). Hypoxia-inducible factor 1α (HIF1α) is critical for the induction of CD39/CD37 in MDSCs, and Met has been shown to inhibit HIF1α through the activation of AMPKα. Another report suggested that Met antagonizes the migration of adoptively transferred MDSCs into tumor xenografts in nude mice through the activation of AMPK, followed by the inhibition of NF-κB (44). Met-induced AMPKα phosphorylation in MDSCs plays a critical role in both observations. In contrast to this research standpoint, in our study we focused on the metabolic profile of $CD11b^+$ myeloid cells, including MDSCs and TAMs, in a syngeneic mouse tumor model.

Analyses of myeloid cell metabolic profiles suggested a unique possibility that metabolism is dependent on cell location. For example, the spleen contains plenty of oxygen and nutrients (e.g. glucose and amino acids). In contrast, the tumor microenvironment is characterized by low oxygen (45), low glucose (46) and low pH (47), all of which dysregulate tumor immunity. Environmental stress may affect metabolic states in each cell population following Met treatment. Indeed, Met up-regulates SRC in splenic myeloid cells, but not in tumor cells. Moreover, Met down-regulates BRC within myeloid cells in tumors, but not in spleens. In this context, the dissection of tumor-derived myeloid cells by incorporation of 2-NBDG and BODIPY® might reveal a link between metabolism and an anti-tumor effect. Met down-regulates BODIPY® incorporation in MDSCs and TAMs, implying the down-regulation of FAO, and hence, OXPHOS. TAMs, such as M2-like macrophages with angiogenic properties, depend on FAO for their metabolism. Met treatment down-regulates the FAO of TAMs while maintaining glycolysis, as indicated by 2-NBDG incorporation, which is important in sustaining tumoricidal effects and is likely involved in non-T-cell- as well as T-cell-dependent anti-tumor activities.

In summary, we demonstrated that Met administration results in decreased numbers of CD11b$^+$ cells and phenotypic alterations in MDSCs and TAMs in tumor-bearing mice, which might contribute to the generation of a T-cell-independent, growth inhibitory effect against certain tumors. Met-induced metabolic reprogramming is critically involved in the phenotypic changes of those cells. This observation gives rise to the possibility of immunotherapy involving Met as an alternative approach for the treatment of osteosarcomas that are refractory to conventional therapies.

Funding

This work was supported by grants from the Japan Agency for Medical Research and Development and the Projects for Development of Innovative Research on Cancer Therapeutics supported by the Ministry of Education, Culture, Sports, Science, and Technology, Japan (15653356 to H.U.) and the Secom Science and Technology Foundation.

Acknowledgements

We thank Ms Yamashita for technical assistance and maintenance of BALB/c SCID mice. T.U., S.E., M.N. and Y.K. designed and performed the experiments. A.Y., T.F., T.K. and T.O. contributed to extensive discussions and critical manuscript reading. H.U. supervised the project, designed the experiments and wrote the paper.

Conflicts of interest statement: The authors declared no conflicts of interest.

References

1 Schlecker, E., Stojanovic, A., Eisen, C. *et al.* 2012. Tumor-infiltrating monocytic myeloid-derived suppressor cells mediate CCR5-dependent recruitment of regulatory T cells favoring tumor growth. *J. Immunol.* 189:5602.
2 Gabrilovich, D. I. and Nagaraj, S. 2009. Myeloid-derived suppressor cells as regulators of the immune system. *Nat. Rev. Immunol.* 9:162.
3 Pollard, J. W. 2004. Tumour-educated macrophages promote tumour progression and metastasis. *Nat. Rev. Cancer* 4:71.
4 Adeegbe, D. O. and Nishikawa, H. 2013. Natural and induced T regulatory cells in cancer. *Front. Immunol.* 4:190.
5 Auffray, C., Fogg, D., Garfa, M. *et al.* 2007. Monitoring of blood vessels and tissues by a population of monocytes with patrolling behavior. *Science* 317:666.
6 Youn, J. I., Nagaraj, S., Collazo, M. and Gabrilovich, D. I. 2008. Subsets of myeloid-derived suppressor cells in tumor-bearing mice. *J. Immunol.* 181:5791.
7 Bronte, V., Brandau, S., Chen, S. H. *et al.* 2016. Recommendations for myeloid-derived suppressor cell nomenclature and characterization standards. *Nat. Commun.* 7:12150.
8 Giaccia, A. J., Simon, M. C. and Johnson, R. 2004. The biology of hypoxia: the role of oxygen sensing in development, normal function, and disease. *Genes Dev.* 18:2183.
9 Nagaraj, S., Gupta, K., Pisarev, V. *et al.* 2007. Altered recognition of antigen is a mechanism of CD8$^+$ T cell tolerance in cancer. *Nat. Med.* 13:828.
10 Rodriguez, P. C., Ernstoff, M. S., Hernandez, C. *et al.* 2009. Arginase I-producing myeloid-derived suppressor cells in renal cell carcinoma are a subpopulation of activated granulocytes. *Cancer Res.* 69:1553.
11 Taketo, M. M. 1998. Cyclooxygenase-2 inhibitors in tumorigenesis (part I). *J. Natl Cancer Inst.* 90:1529.
12 Bertagnolli, M. M. 2007. Chemoprevention of colorectal cancer with cyclooxygenase-2 inhibitors: two steps forward, one step back. *Lancet Oncol.* 8:439.
13 Stein, M., Keshav, S., Harris, N. and Gordon, S. 1992. Interleukin 4 potently enhances murine macrophage mannose receptor activity: a marker of alternative immunologic macrophage activation. *J. Exp. Med.* 176:287.
14 Mills, C. D. 2012. M1 and M2 macrophages: oracles of health and disease. *Crit. Rev. Immunol.* 32:463.
15 Lewis, J. S., Landers, R. J., Underwood, J. C., Harris, A. L. and Lewis, C. E. 2000. Expression of vascular endothelial growth factor by macrophages is up-regulated in poorly vascularized areas of breast carcinomas. *J. Pathol.* 192:150.
16 Sunderkötter, C., Steinbrink, K., Goebeler, M., Bhardwaj, R. and Sorg, C. 1994. Macrophages and angiogenesis. *J. Leukoc. Biol.* 55:410.
17 Mantovani, A., Sozzani, S., Locati, M., Allavena, P. and Sica, A. 2002. Macrophage polarization: tumor-associated macrophages as a paradigm for polarized M2 mononuclear phagocytes. *Trends Immunol.* 23:549.
18 Ruffell, B., Chang-Strachan, D., Chan, V. *et al.* 2014. Macrophage IL-10 blocks CD8$^+$ T cell-dependent responses to chemotherapy by suppressing IL-12 expression in intratumoral dendritic cells. *Cancer Cell* 26:623.
19 Leek, R. D. and Harris, A. L. 2002. Tumor-associated macrophages in breast cancer. *J. Mammary Gland Biol. Neoplasia* 7:177.
20 Nishie, A., Ono, M., Shono, T. *et al.* 1999. Macrophage infiltration and heme oxygenase-1 expression correlate with angiogenesis in human gliomas. *Clin. Cancer Res.* 5:1107.
21 Lin, E. Y., Nguyen, A. V., Russell, R. G. and Pollard, J. W. 2001. Colony-stimulating factor 1 promotes progression of mammary tumors to malignancy. *J. Exp. Med.* 193:727.
22 Coussens, L. M., Zitvogel, L. and Palucka, A. K. 2013. Neutralizing tumor-promoting chronic inflammation: a magic bullet? *Science* 339:286.
23 Quail, D. F. and Joyce, J. A. 2013. Microenvironmental regulation of tumor progression and metastasis. *Nat. Med.* 19:1423.
24 Strachan, D. C., Ruffell, B., Oei, Y. *et al.* 2013. CSF1R inhibition delays cervical and mammary tumor growth in murine models by attenuating the turnover of tumor-associated macrophages and enhancing infiltration by CD8+ T cells. *Oncoimmunology* 2:e26968.
25 Kelly, B. and O'Neill, L. A. 2015. Metabolic reprogramming in macrophages and dendritic cells in innate immunity. *Cell Res.* 25:771.
26 Krawczyk, C. M., Holowka, T., Sun, J. *et al.* 2010. Toll-like receptor-induced changes in glycolytic metabolism regulate dendritic cell activation. *Blood* 115:4742.
27 Pantel, A., Teixeira, A., Haddad, E., Wood, E. G., Steinman, R. M. and Longhi, M. P. 2014. Direct type I IFN but not MDA5/TLR3 activation of dendritic cells is required for maturation and metabolic shift to glycolysis after poly IC stimulation. *PLoS Biol.* 12:e1001759.
28 Doyle, A. G., Herbein, G., Montaner, L. J. *et al.* 1994. Interleukin-13 alters the activation state of murine macrophages *in vitro*: comparison with interleukin-4 and interferon-gamma. *Eur. J. Immunol.* 24:1441.
29 Mills, C. D., Kincaid, K., Alt, J. M., Heilman, M. J. and Hill, A. M. 2000. M-1/M-2 macrophages and the Th1/Th2 paradigm. *J. Immunol.* 164:6166.
30 Eikawa, S., Nishida, M., Mizukami, S., Yamazaki, C., Nakayama, E. and Udono, H. 2015. Immune-mediated antitumor effect by type 2 diabetes drug, metformin. *Proc. Natl Acad. Sci. USA* 112:1809.
31 Kunisada, Y., Eikawa, S., Tomonobu, N. *et al.* 2017. Attenuation of CD4$^+$CD25$^+$ regulatory T cells in the tumor microenvironment by metformin, a Type 2 diabetes drug. *EBioMedicine* 25:154.
32 Memmott, R. M., Mercado, J. R., Maier, C. R., Kawabata, S., Fox, S. D. and Dennis, P. A. 2010. Metformin prevents tobacco carcinogeninduced lung tumorigenesis. *Cancer Prev. Res.* 3:1066.
33 Ugel, S., De Sanctis, F., Mandruzzato, S. and Bronte, V. 2015. Tumor-induced myeloid deviation: when myeloid-derived suppressor cells meet tumor-associated macrophages. *J. Clin. Invest.* 125:3365.
34 Rose, S., Misharin, A. and Perlman, H. 2012. A novel Ly6C/Ly6G-based strategy to analyze the mouse splenic myeloid compartment. *Cytometry A* 81:343.

35 Wang, B., Li, Q., Qin, L., Zhao, S., Wang, J. and Chen, X. 2011. Transition of tumor-associated macrophages from MHC class II^{hi} to MHC class II^{low} mediates tumor progression in mice. *BMC Immunol.* 12:43.
36 Gundra, U. M., Girgis, N. M., Ruckerl, D. *et al.* 2014. Alternatively activated macrophages derived from monocytes and tissue macrophages are phenotypically and functionally distinct. *Blood* 123:e110.
37 Olsson, A., Nakhlé, J., Sundstedt, A. *et al.* 2015. Tasquinimod triggers an early change in the polarization of tumor associated macrophages in the tumor microenvironment. *J. Immunother. Cancer* 3:53.
38 Wang, J. C., Sun, X., Ma, Q. *et al.* 2018. Metformin's antitumour and anti-angiogenic activities are mediated by skewing macrophage polarization. *J. Cell. Mol. Med.* 22:3825.
39 Roberts, S. S., Chou, A. J. and Cheung, N. K. 2015. Immunotherapy of childhood sarcomas. *Front. Oncol.* 5:181.
40 Gordon, S. R., Maute, R. L., Dulken, B. W. *et al.* 2017. PD-1 expression by tumour-associated macrophages inhibits phagocytosis and tumour immunity. *Nature* 545:495.
41 Scharping, N. E., Menk, A. V., Whetstone, R. D., Zeng, X. and Delgoffe, G. M. 2017. Efficacy of PD-1 blockade is potentiated by metformin-induced reduction of tumor hypoxia. *Cancer Immunol. Res.* 5:9.
42 Movahedi, K., Laoui, D., Gysemans, C. *et al.* 2010. Different tumor microenvironments contain functionally distinct subsets of macrophages derived from Ly6C(high) monocytes. *Cancer Res.* 70:5728.
43 Li, L., Wang, L., Li, J. *et al.* 2018. Metformin-induced reduction of CD39 and CD73 blocks myeloid-derived suppressor cell activity in patients with ovarian cancer. *Cancer Res.* 78:1779.
44 Qin, G., Lian, J., Huang, L. *et al.* 2018. Metformin blocks myeloid-derived suppressor cell accumulation through AMPK-DACH1-CXCL1 axis. *Oncoimmunology* 7:e1442167.
45 Theurich, S., Rothschild, S. I., Hoffmann, M. *et al.* 2016. Local tumor treatment in combination with systemic ipilimumab immunotherapy prolongs overall survival in patients with advanced malignant melanoma. *Cancer Immunol. Res.* 4:744.
46 Chang, C. H., Qiu, J., O'Sullivan, D. *et al.* 2015. Metabolic competition in the tumor microenvironment is a driver of cancer progression. *Cell* 162:1229.
47 Brand, A., Singer, K., Koehl, G. E. *et al.* 2016. LDHA-associated lactic acid production blunts tumor immunosurveillance by T and NK cells. *Cell Metab.* 24:657.